Original Article

The Possible Role of Folic Acid Against Sodium Fluoride Induced Toxicity in the Skin of Adult Male Albino Rats

Heba Kamal Mohamed and Rasha Ibrahim Anwar

Department of Human Anatomy and Embryology, Faculty of Medicine, Assiut University, Egypt

ABSTRACT

Background: Exposure of human being to fluoride occurs through various sources as food, water, toothpastes and fluoride additives. This exposure is either to low concentrations for long periods or to high concentrations and both may lead to poisoning. Folic acid (FA) has an important free radical scavenging property which makes it the most potent antioxidants. Moreover, it suppresses apoptosis and boost cell survival.

Aim of the Work: To evaluate the protective and therapeutic role of FA against sodium fluoride (NaF) induced toxicity on adult male rat skin.

Materials and Methods: Forty adult (3 months) male albino rats (weighing 200-220 gm) were equally divided into 4 groups (10 rats each): group 1 (control), group 2 (NaF, for 4 weeks), group 3 (NaF, for 4 weeks followed by FA for another 4 weeks) and group 4 (NaF plus FA for 4 weeks). Both NaF (25mg/Kg b.w.) and FA (8 mg/Kg b.w.) were given orally daily. The rats were sacrificed and samples of the back skin were processed for histological, immunohistochemical (Bcl2 antiapoptotic protein) and morphometric studies.

Results: Group 2 revealed signs of degeneration in epidermal cells, expansion of intercellular spaces and destructed organelles. There was a reduction in epidermal thickness with disturbance in collagen fibers arrangement and weak immunoreactivity of Bcl-2. FA induced relative improvement in the dermal and epidermal structures in group 3 while there was preservation of these structures in group 4.

Conclusion: FA ameliorates NaF induced harmful effects on skin in addition to its valuable preventive role.

Received: 15 April 2019, **Accepted:** 26 May 2019

Key Words: FA, NaF, rat, skin.

Corresponding Author: Heba K. Mohamed, Department of Human Anatomy and Embryology, Faculty of Medicine, Assiut University, Egypt, **Tel.:** +20 10 0101 6547, **E-mail:** hebaelgamae73@yahoo.com

The Egyptian Journal of Anatomy, ISSN: 0013-2446, Vol. 42 No. 2

INTRODUCTION

Medicine, in particular dentistry, agriculture and industry are from the most common fields in which fluoride compounds have been used[1]. Exposure of human to fluoride occurs through various sources as food, water, toothpastes, fluoride additives, and use of fluoride gel[2]. Fluorides also are used in rodenticides, phosphate fertilizers, ceramics and brick industries[3].

Exposure to fluoride in high concentrations or low concentrations for long time in water or in foods may lead to fluoride poisoning Fluorosis[4]. Fluoride overexposure may result in many dramatic effects as chronic dental or skeletal fluorosis or acute poisoning which can threaten the life[5,6].

Fluoride contradicts with dental plaque microorganisms' formation, and increases the durability of mineralized tissues against acid demineralization. In addition; lung, skin, and kidney epithelia are often exposed and affected by fluoride[7]. Collagen and cells of the connective tissue which constitute the organic part of supporting tissues are also affected by fluorine compounds, as these compounds increase the non-collagen proteins mass and thus promote the skin aging[1]. Moreover, fluoride inhibits collagen biosynthesis in tissues such as bone, tendon, tracheal rings and skin[8]. Although; epithelium especially keratinocytes are often exposed to fluoride However, effects of fluoride on these cells remain non investigated to a great extent[7]. It was reported that, oxidative stress induced by sodium

 DOI: 10.21608/ejana.2019.10703.1016

fluoride is the main cause for cell degeneration and apoptosis[4].

Folic acid (FA) is a synthetic form of folate (vitamin B9) which presents as supplements and in many enriched foods[9]. It is a powerful antioxidant as it has a free radical scavenging property[10]. It promotes cell survival and suppresses apoptosis[11].

Aging is a gradual cumulative process that occurs in all organs. The modifications in apoptosis may take part in these age-associated changes. Bcl-2 is a protein which has antiapoptotic activity in response to a various stimuli[12]. The role of Bcl-2 in controlling cell survival and death have been focused by many researchers[13].

The aim of this work was to detect the role of folic acid in amelioration of the hazardous effects of sodium fluoride on the skin and its possible protective effects.

MATERIALS AND METHODS

Animals

In this study, 40 adult (3 months) male albino rats (weighing 200-220 gm) were used, obtained from Animal House, Faculty of Medicine, Assuit University. The rats were fed with commercial rat chow and had free access to food and water. Room temperature was kept at 23± 3 Cº with constant daily light/dark cycle throughout the experiment. The internationally accepted principles for the care and use of laboratory animals were followed in this study.

Chemicals

- Sodium fluoride (NaF) and folic acid (FA) were obtained from Sigma (St. Louis, Mo, USA).
- Bcl-2 (B-cell lymphoma 2) was purchased from US Biological Company, United States.
- Other chemicals were of high analytical grades.

Experimental design

4 groups were used in this study (10 rats each):

- **Group 1 (control):** Rats received distilled water.
- **Group 2 (NaF-treated group):** 25mg/Kg b.w. NaF was given to rats orally (dissolved in distilled water) daily for 4 weeks[14].
- **Group 3 (treated with NaF followed by FA) (therapeutic group):** NaF with the previous dose (25mg/Kg b.w.) was given to rats for 4 weeks then stopped and rats received FA 8mg/Kg b.w. orally (dissolved in distilled water) daily for another 4 weeks[15].
- **Group 4 (treated with NaF + FA) (protected group):** NaF (25mg/Kg b.w.) concurrently with FA (8mg/Kg b.w.) were given to rats for 4 weeks.

Tissue sampling

The rats of each group at the end of the experiment were anesthetized by ether; the hair over an area 2x2 cm on the back is shaved. Then, the rats sacrificed, their hearts were perfused with isotonic saline through the left ventricle until the flowing blood was cleared. The prepared areas of the skin were taken, treated for a histological and an immunohistochemical study.

Histological study

For light microscopic study, immersion of the specimens into formaldehyde solution (10%) was done, treated and embedded in paraffin and cut serially (5µm-thickness), then Hematoxylin and eosin (H&E) and Masson's trichrome staining were done[16].

For ultrastructural study, small pieces (1mm) of the skin were cut and fixed in 2.5% phosphate buffered gluteraldehyde, treated for semithin sections (0.5-1µm) and stained with toluidine blue. Ultrathin sections (80-90 nm) were cut with ultramicrotome and stained with uranyl acetate and lead citrate[17], then photographed by transmission electron microscope (Jeol-JEM-100 CXII Jeol, Tokyo, Japan) in the Electron Microscopic Unit, Assiut University.

Immunohistochemical study

Immunohistochemical staining for detection of the antiapoptotic protein Bcl2 (B-cell lymphoma-2), the primary antibody used was rabbit polyclonal antibody. The cellular reaction was cytoplasmic[18].

Immunohistochemical study was conducted using the avidin–biotin peroxidase method. Paraffin sections were deparaffinized, rehydrated in descending grades of alcohol, and incubated over night with the primary antibody (diluted 1:100) at 4°C. Phosphate-buffered saline (PBS) was used for rinsing the sections three times then

incubated for 1hour with peroxidase-conjugated secondary antibody and washed three times with PBS. The immunoreactivity was visualized by using 3,3′-diaminobenzidine hydrogen peroxide as a chromogen. Finally, counterstaining to slides with Mayer's hematoxylin was done[19]. Replacing primary antibody with buffer or non immune serum was performed for negative controls[13]. The positive control was tonsil. Immunohistochemical staining was done at Faculty of Medicine, Assiut University.

Morphometric and statistical study

Using the image analyzer computer system Leica Qwin 500 Ltd image analysis computer system Wetzlar, Germany, the following measurements were done:

1. Epidermal thickness using H&E stain.
2. Area% of collagen fibers using Masson's trichrome stain.
3. The percent of mean area of expression of Bcl-2 immunoreactivity.

The measurements were carried out in five non-overlapping high power fields in five randomly chosen sections in the studied groups using an objective lens X400.

All measurements were done per area of the view field. Data in all groups were statistically analyzed using SPSS (version13) statistical package. Mann-Whitney test was used and the resulting data expressed as mean ± standard deviation. *P value* was considered significant when it is less than 0.05. *P value* of less than 0.001 was considered highly significant.

RESULTS

I. Histological results

A. Light microscopic results

1- Hematoxylin and Eosin stain (H&E)

In control (group 1) examination of stained sections showed the two layers of the skin; epidermis and underlying dermis. Adipose connective tissue layer; the hypodermis is seen beneath the dermis. Epidermis appeared as arranged layers of stratified keratinocytes; stratum basale resting on a basement membrane, the stratum spinosum, the stratum granulosum, and the stratum corneum. An upper papillary and lower reticular layers are the constituent of the dermis. It contained hair follicles with associated sebaceous glands (Figures 1a,b). While group 2 sections showed that the epidermal thickness was apparently reduced when compared to the control. Nuclei with deep staining and pale vacuolated cytoplasm could be seen in some keratinocytes. The dermis showed disturbed collagen fibers, empty vacuolated areas, few connective tissue cells, congested and dilated dermal capillaries, cellular infiltration and multinucleated cells (Figures 2a,b). In group 3, thin epidermal thickness is still seen compared to the control group. Few cells with deeply stained nuclei and pale vacuolated cytoplasm were seen. The dermis had some areas of vacuolations and cellular infiltrations (Figures 3a,b). Sections of the skin in group 4 showed that most of epidermal cells and dermis maintained their normal appearance with preserved the thickness of the epidermis compared to the groups 2 &3 (Figure 4a,b).

2- Masson's trichrome stain

Group 1 showed abundant coarse greenish interwoven collagen fibers in the dermis (Figure 5). However, in group 2 there was a remarkable decrease, fragmentation, disorganization and wide separation of the collagen fibers with many empty spaces (Figure 6). In group 3, the collagen fibers were still disorganized with some empty spaces (Figure 7); meanwhile, in group (4) the collagen fibers appeared nearly similar to the control (Figure 8).

3- Immunohistochemical stain

Bcl-2 immunostained sections in group 1 revealed a strong brownish Bcl-2 expression mainly in basal epidermal cells and in some connective tissue cells in the dermis (Figure 9). In group 2, a weak Bcl-2 immuno-expression was observed (Figure 10), while in group 3, the reaction was mild (Figure 11). In group 4, positive Bcl-2 expression which is nearly similar to the control group was detected in the basal epidermal and dermal cells (Figure 12).

4- Toluidine blue stain

Semithin sections in group 1 showed the different epidermal cells layers and the underlying dermis. The intercellular spaces between the epidermal cells could be clearly seen. The basal layer revealed columnar cells with oval nuclei, while the spinous layer cells had short cytoplasmic projections. Granular layer cells had deeply basophilic granules and the overlying horny layer which formed of keratinized flattened non-nucleated cells (Figure 13). However in

group 2, widened intercellular spaces between the epidermal cells and a reduction in the epidermal thickness could be clearly detected. Moreover, vacuolated areas could be seen surrounding some epidermal cells and other cells had pale or deeply stained irregular nucleus. The dermis showed disorganization of connective tissue and many empty spaces (Figure 14). Toluidine blue-stained sections in group 3 revealed areas with a widened intercellular space between keratinocytes, while other cells with a normal intercellular space. Some epidermal cells had cytoplasmic vacuolation. The dermis appeared normal to a great extent (Figure 15). In group 4, the epidermis and the dermis appeared nearly similar to the control. Moreover, the epidermal layer thickness and intercellular spaces between the keratinocytes were clearly seen similar to the control (Figure 16).

B. Ultrastructural results

The skin ultrathin sections in group 1 showed the basal keratinocytes resting on a basement membrane with a large rounded nucleus. Mitochondria and free ribosomes could be seen in the cytoplasm. The adjacent spinous cell had an oval nucleus, free ribosomes, tonofilaments and mitochondria in the cytoplasm. Intact desmosomal junctions could be seen connecting the cells (Figures 17,18). The underlying dermal collagen fibers appeared regular. Spindle shaped fibroblast with an oval elongated euchromatic nucleus, rough endoplasmic reticulum and free ribosomes in the cytoplasm could be seen (Figure 19).

Epidermal ultrathin sections in group 2 showed basal and spinous cells with heterochromatic highly folded nuclei. There was disruption of desmosomes with widened intercellular space (Figure 20). Peripheral chromatin condensation in the nucleus could be seen in some basal cells. Other cells had an electron dense shrunken, irregular nucleus with perinuclear halos. Vacuolated mitochondria inside the darkly stained cytoplasm, widening of intercellular spaces and disruption of desmosomal junctions could be also seen (Figure 21). Some spinous cells appeared shrunken with an apoptotic nucleus and a wide intercellular space. Other cells revealed cytoplasmic vacuolations and dilated cisternae of rough endoplasmic reticulum with dense particles in some of them (Figure 22). The nucleus of fibroblast was deeply stained, finely granulated with irregular nuclear membrane. It was surrounded by densely stained scanty cytoplasm with unidentifiable cellular organelles. Basal keratinocytes with dilated rough endoplasmic reticulum cisternae which contain dense particles were observed overlying the basement membrane. Disorganization in the underlying collagen bundles appeared clearly (Figure 23).

In group 3, basal epidermal cells could be seen resting on their basement membrane with euchromatic nucleus and deeply stained cytoplasm which revealed rough endoplasmic reticulum dilated cisternae which contained dense particles. The adjacent spinous cells had an oval euchromatic nucleus and a little amount of tonofilaments. Desmosomes with adjacent cells were noticed. The intercellular space was seen widened in some areas. Some basal cells had irregular indented nucleus (Figures 24,25). Fibroblast showed oval elongated nucleus surrounded with cytoplasm contained vacuolated mitochondria and many electron dense bodies. Collagen bundles could be seen in the underlying dermis (Figure 26).

Examination of the ultrathin sections in group 4 showed that the basal keratinocytes and adjacent spinous cells revealed euchromatic nuclei and appeared similar to the normal to a great extent. In some areas, slight widening of intercellular spaces was seen (Figure 27). The fibroblast appeared more or less similar to the control with its oval elongated nucleus; rough endoplasmic reticulum and free ribosomes in the cytoplasm. However, some vacuolated mitochondria could be observed (Figure 28).

II- Morphometric and statistical results

Using Mann-Whitney test, the epidermal thickness showed a significant decrease in groups 2&3 compared to the control. At the same time, it increased significantly in groups 3 and 4 as compared to group 2, while the difference in the epidermal thickness between group 4 and group 1 was a non-significant (Table 1, Histogram 1).

The area% of collagen fibers decreased significantly in groups 2&3 when compared to group 1. In groups 3 and 4, the increase in area% of the collagen fibers was significant as compared to group 2. The difference between group 4 & group 1 was a non-significant (Table 2, Histogram 2).

Regarding the area% of Bcl-2 expression, the decrease was significant in group 2 comparing to group 1. However, the difference in groups 3 and 4 was a non-significant as compared to group 1. Meanwhile, the increase was significant in groups 3&4 in comparison with group 2 (Table 3, Histogram 3).

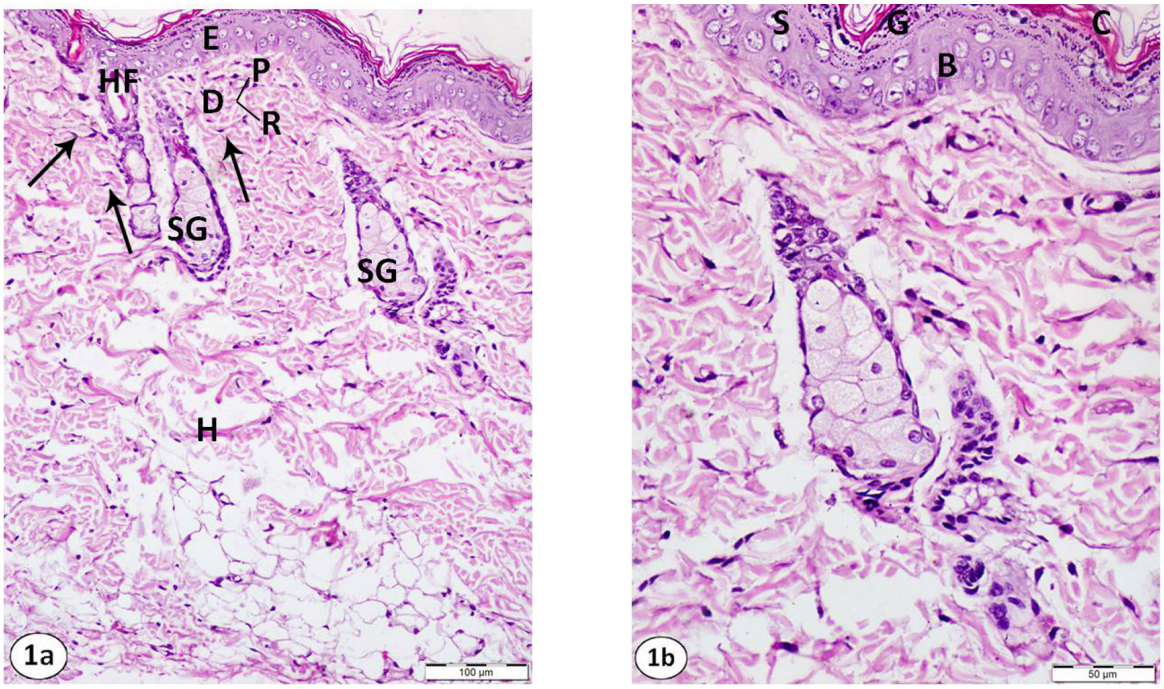

Fig. 1: Photomicrographs of skin sections of an adult control rat (group 1) showing: (1a) Normal skin structure; epidermis (E), dermis (D) with upper papillary (P) and lower reticular (R) layers and hypodermis of adipose tissue (H). Many connective tissue cells with spindle shaped nuclei (arrows), Hair follicles (HF) with associated sebaceous glands (SG) can be seen in the dermis. (1b) The layers of the stratified epidermis; stratum basale (B) on basement membrane, stratum spinosum (S), stratum granulosum (G) and stratum corneum (C). H&E, (1a): X200, (1b): X400.

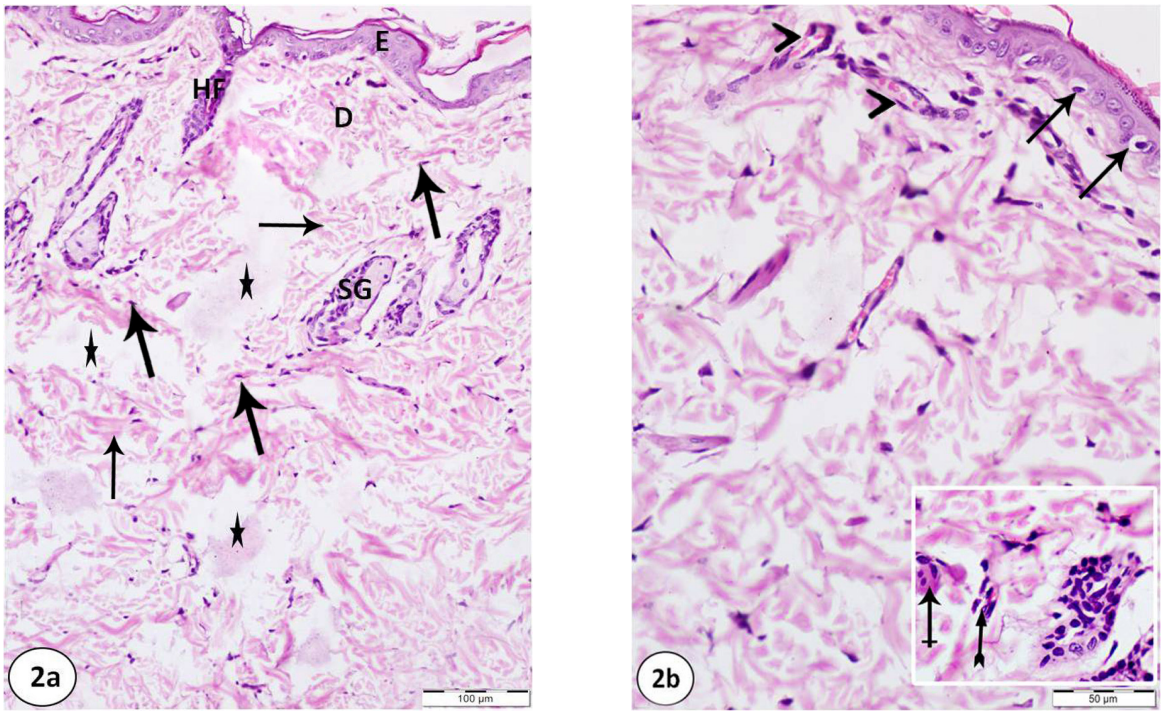

Fig. 2: Photomicrographs of skin sections of an adult rat (group 2) showing: (2a) The epidermis (E) with apparent decrease in its thickness. Disorganized collagen fibers (thin arrows), vacuolated areas (stars) and few connective tissue cells (thick arrows) could be seen in the dermis (D). Hair follicles (HF) and sebaceous glands (SG) can be also seen. (2b) Epidermal cells with cytoplasmic vacuolation and deeply stained nuclei (arrows). Congested and dilated dermal capillaries (arrow heads) are noticed. Inset: Showing cellular infiltration (tailed arrow) and multinucleated giant cell (crossed arrow). H&E, (2a): X200, (2b): X400.

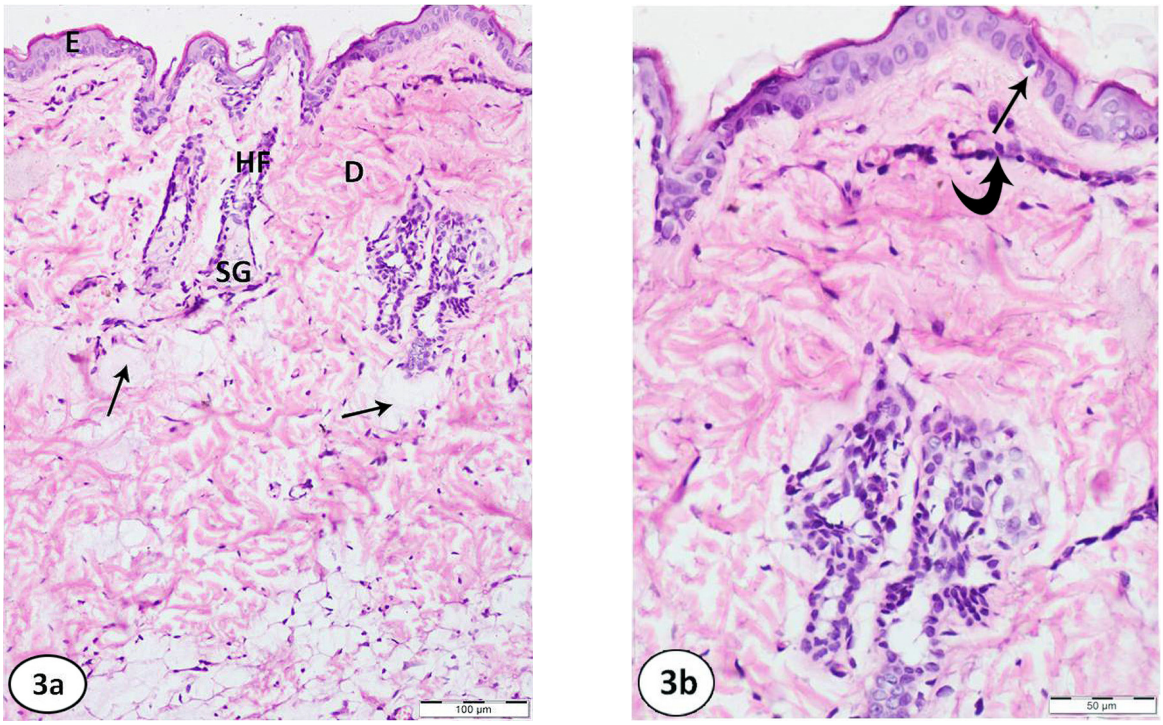

Fig. 3: Photomicrographs of skin sections of an adult rat (group 3) showing: (3a) The epidermis (E) which is apparently still thin. The dermis shows areas of vacuolations (arrows). Hair follicles (HF) and sebaceous glands (SG) can be observed. (3b) Few cells in epidermis can be seen with deeply stained nuclei and surrounded by pale vacuolated cytoplasm (arrow). Note cellular infiltration (curved arrow). H&E, (3a): X200, (3b): X400.

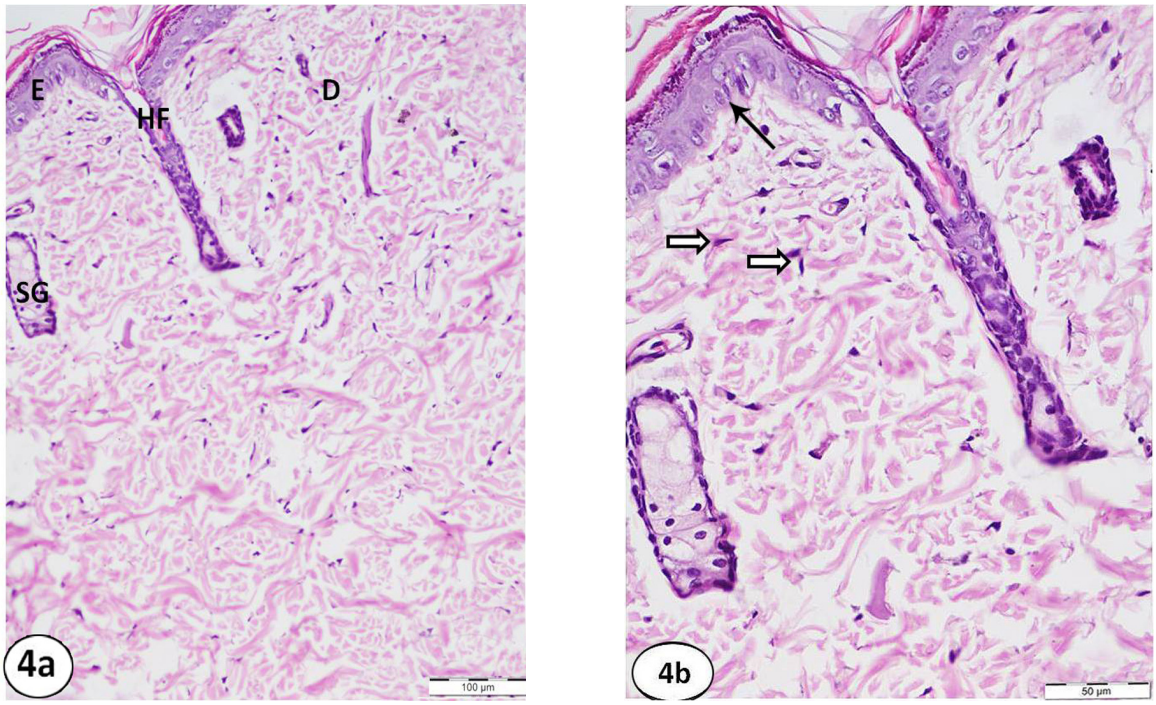

Fig. 4: Photomicrographs of skin sections of adult rat (group 4) showing: (4a) nearly normal skin structure with apparent increase in thickness of epidermis (E) which is more or less similar to the control. The dermis (D), hair follicles (HF) with sebaceous glands (SG) appear normal. (4b) Most cells in epidermis have vesicular nuclei and appear similar to control to a great extent (arrow). Connective tissue cells with spindle shaped nuclei are noticed (open arrows). H&E, (4a): X200, (4b): X400.

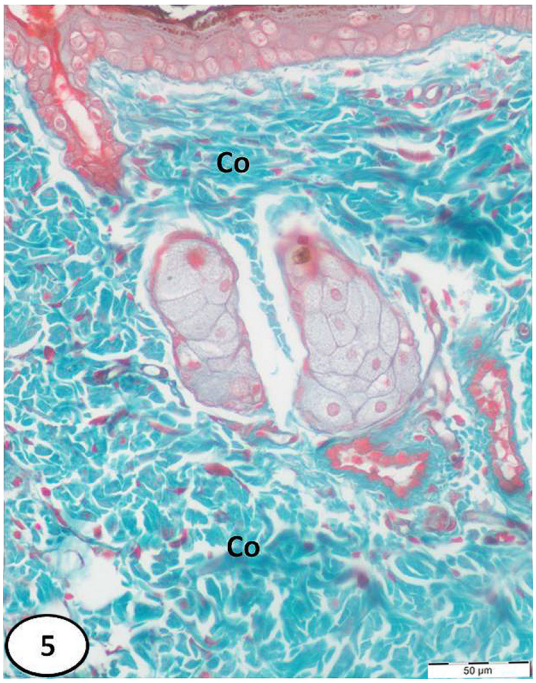

Fig. 5: A photomicrograph of a skin section of adult rat (group 1) showing abundant coarse collagen fibers in the dermis (Co). Masson's trichrome, X400.

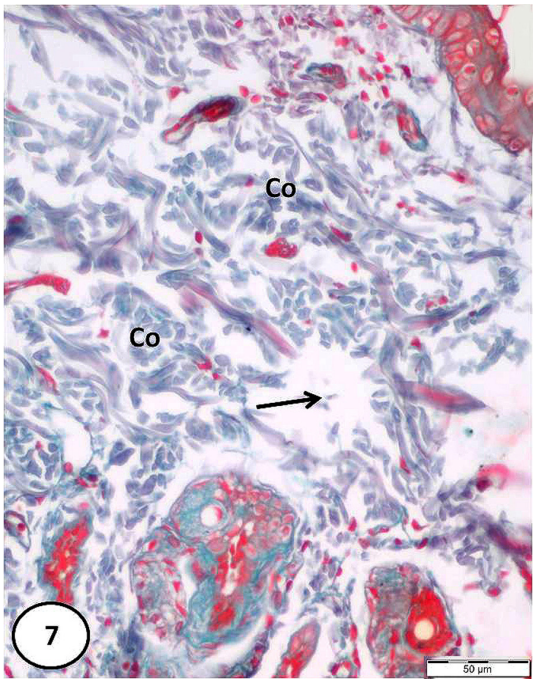

Fig. 7: A photomicrograph of a skin section of adult rat (group 3) showing fine disorganized collagen fibers (Co). Some empty spaces are seen (arrow). Masson's trichrome, X400.

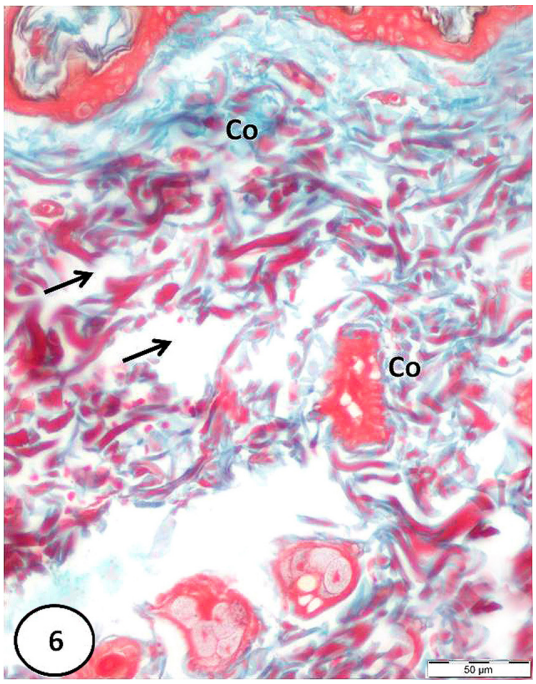

Fig. 6: A photomicrograph of a skin section of adult rat (group 2) showing a dramatic decrease, disorganization and wide separation of the dermal collagen fibers (Co). Many empty spaces can be detected (arrows). Masson's trichrome, X400.

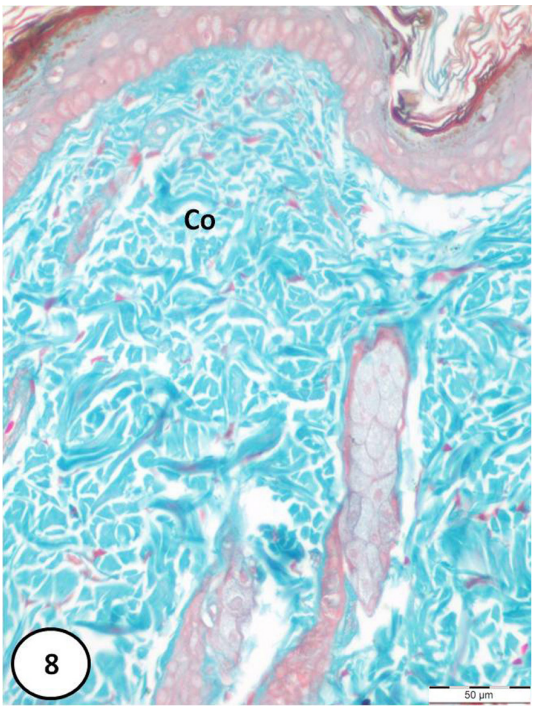

Fig. 8: A photomicrograph of a skin section of adult rat (group 4) showing nearly normal collagen fibers (Co) which looks like the control group. Masson's trichrome, X 400.

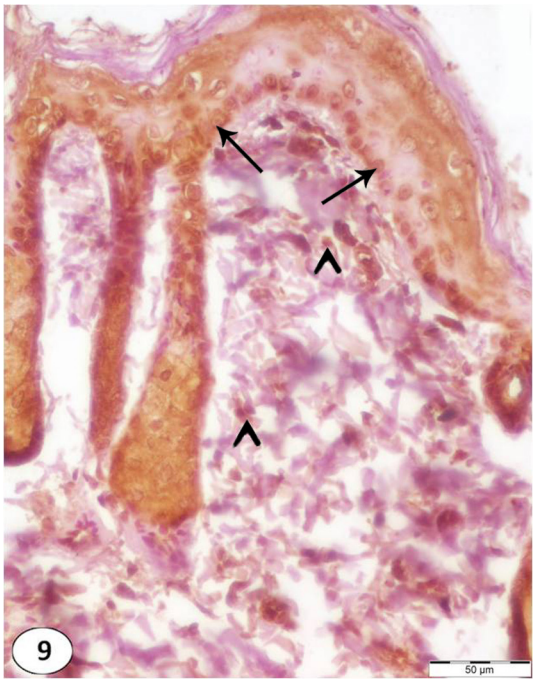

Fig. 9: A photomicrograph of a skin section of adult rat (group 1) showing strong positive immounoexpression of Bcl-2 in the basal epidermal cells (arrows) and some dermal cells (arrow heads). Bcl-2, X 400.

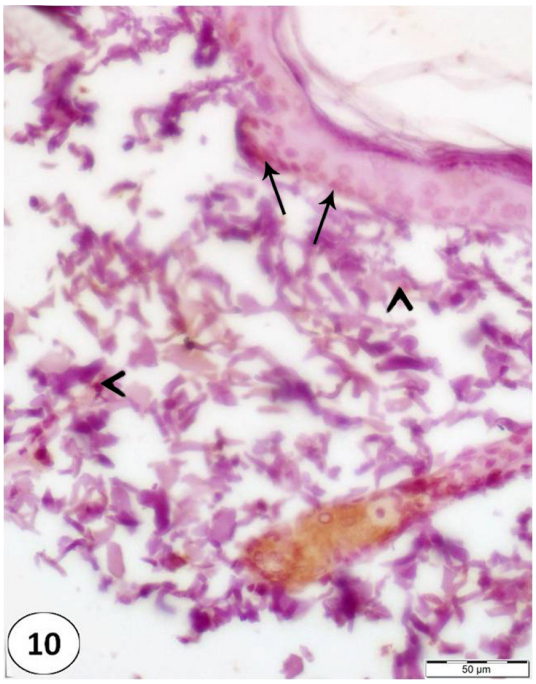

Fig. 10: A photomicrograph of a skin section of adult rat (group 2) showing a weak Bcl-2 immunoexpression in the basal epidermal cells (arrows) and a few dermal connective tissue cells (arrow heads). Bcl2, X400.

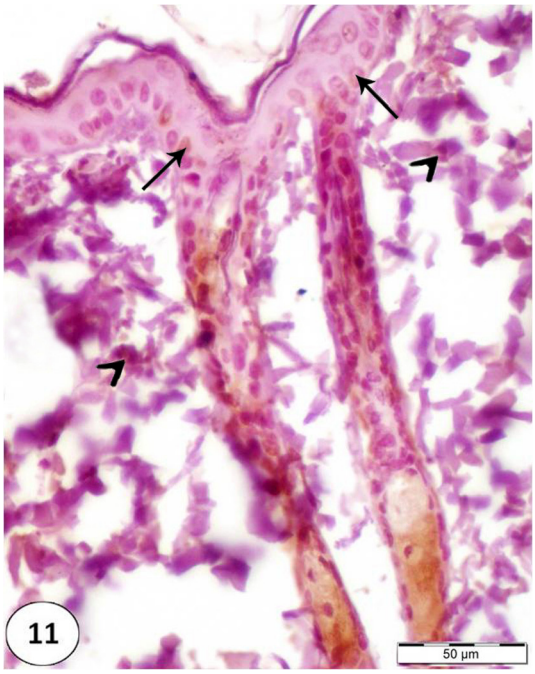

Fig. 11: A photomicrograph of A skin section of adult rat (group 3) showing mild Bcl-2 immunoexpression in basal epidermal cells (arrows) and few dermal cells (arrow heads). Bcl-2, X 400.

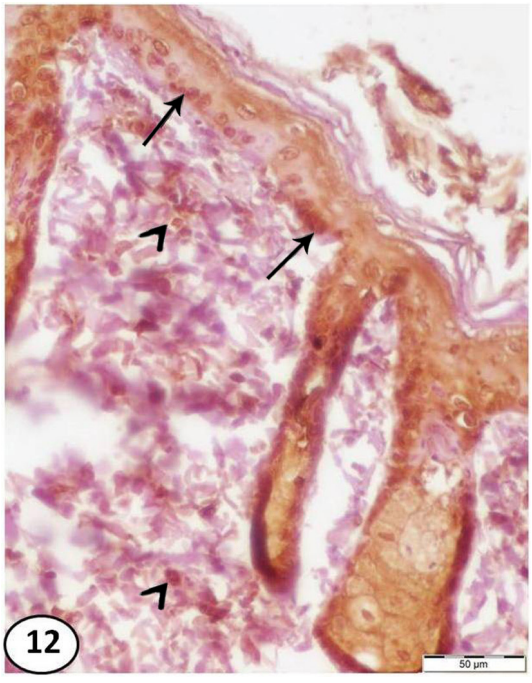

Fig. 12: A photomicrograph of a skin section of adult rat (group 4) showing a positive Bcl-2 immunoexpression which is nearly similar to the control in basal epidermal cells (arrows) and dermal cells (arrow heads). Bcl-2, X 400.

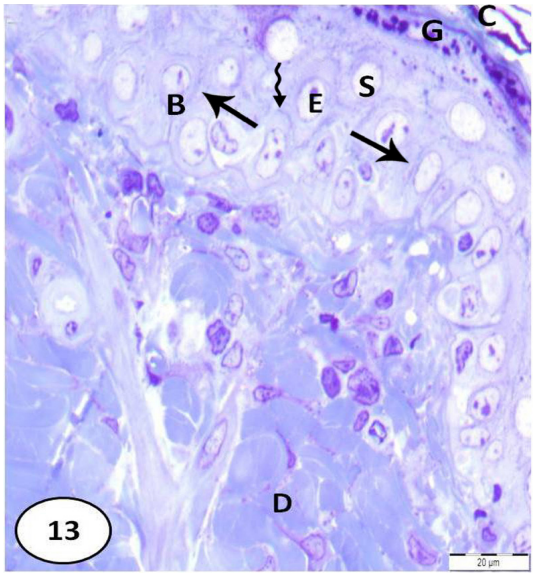

Fig. 13: A photomicrograph of a skin section of adult rat (group 1) showing the different layers of cells in epidermis (E). The layer of stratum basale (B) reveals low columnar cells and oval nuclei with narrow intercellular spaces between the keratinocytes (arrows). The cells of stratum spinosum (S) are seen with short cytoplasmic projections (wavy arrow). The cells of stratum granulosum (G) appear with deeply basophilic granules and the overlying stratum corneum (C) is formed of layers of flattened non-nucleated keratinized cells. The underlying dermis (D) is seen. Toluidine blue, X1000.

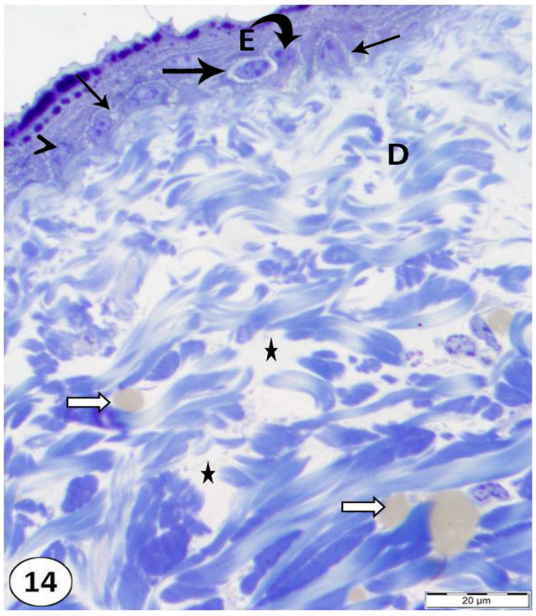

Fig. 14: A photomicrograph of a skin section of adult rat (group 2) showing the cells in epidermis (E) with wide intercellular space (thin arrows). Cells surrounded with vacuolated cytoplasm (thick arrow), others have deeply stained irregular nuclei (curved arrow) or pale nuclei (arrow head) can be seen. Note that there is a marked reduction in the epidermal thickness. The dermis (D) shows many vacuolated areas (stars) and lipid droplets (open arrows). Toluidine blue, X1000.

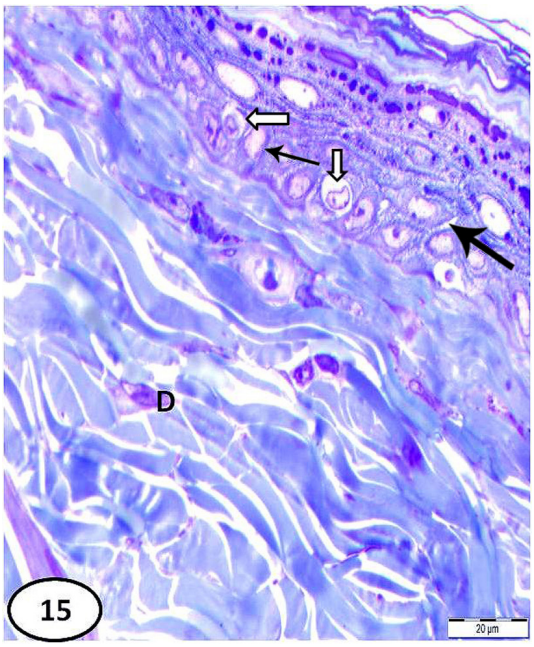

Fig. 15: A photomicrograph of a skin section of adult rat (group 3) showing areas with widened intercellular space between the keratinocytes (thick arrow), while others with normal intercellular space (thin arrow). Some cells reveal cytoplasmic vacuolation (open arrows). The dermis appears more or less normal (D). Toluidine blue, X1000.

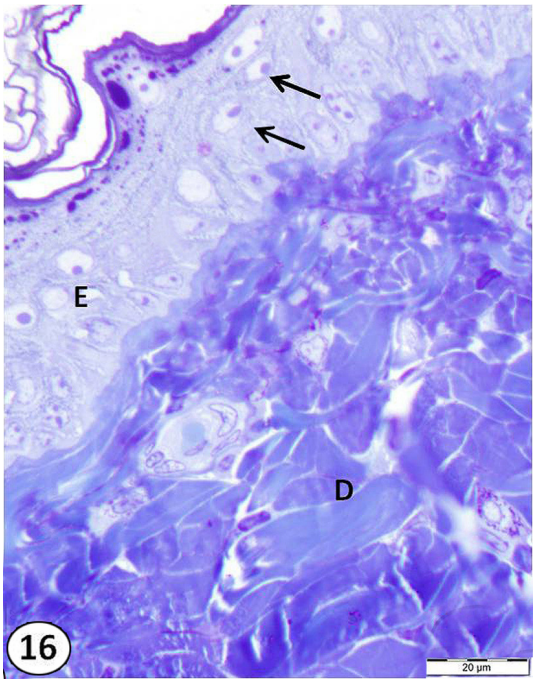

Fig. 16: A photomicrograph of a skin section of adult rat (group 4) showing epidermis (E) and dermis (D) which are nearly similar to the control. Most epidermal cells preserve their layer thickness with nearly normal appearance. Keratinocytes are separated by narrow intercellular spaces (arrows). Toluidine blue, X1000.

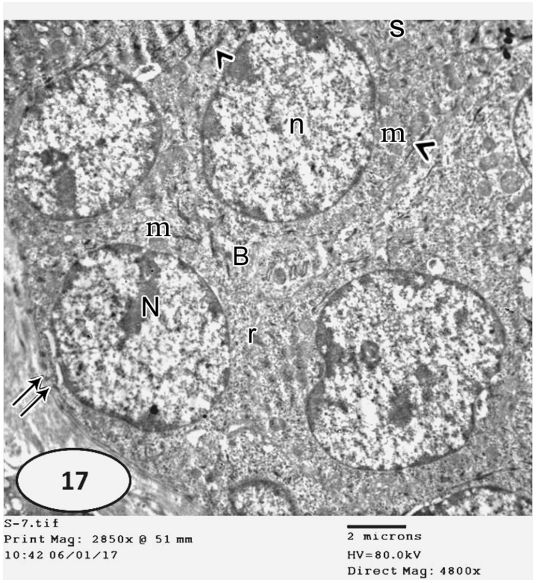

Fig. 17: An electron micrograph of an ultrathin skin section of adult rat (group 1) showing basal keratinocytes (B) resting on a basement membrane (double arrow) with a large rounded nucleus (N). The cytoplasm contains mitochondria (m) and free ribosomes (r). Note the adjacent spinous cell (S) with a large euchromatic oval nucleus (n) and mitochondria (m) in the cytoplasm. Intact desmosomal junctions between adjacent cells (arrow heads) can be seen. TEM, X 4800.

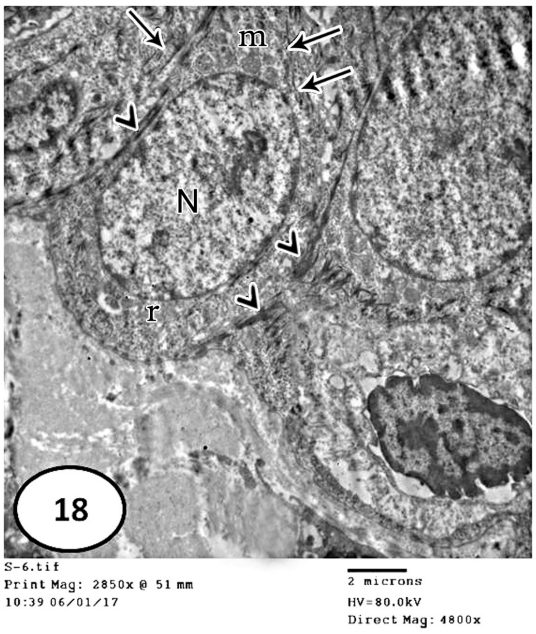

Fig. 18: An electron micrograph of an ultrathin skin section of adult rat (group 1) showing a spinous cell with an oval nucleus (N). Mitochondria (m), tonofilaments (arrows) and free ribosomes (r) can be seen in the cytoplasm. Desmosomes are clearly seen (arrow heads). TEM, X 4800.

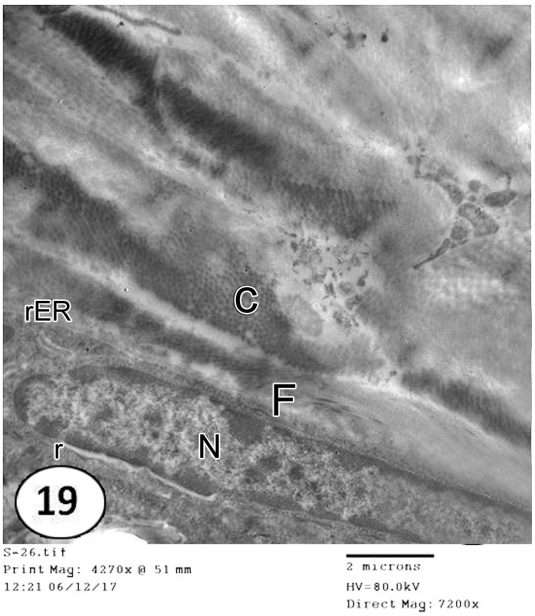

Fig. 19: An electron micrograph of an ultrathin skin section of adult rat (group 1) showing a spindle shaped fibroblast (F) with an oval elongated euchromatic nucleus (N). Rough endoplasmic reticulum (rER) and free ribosomes (r) could be seen in the cytoplasm. Note underlying regular collagen fibers in the dermis (C). TEM, X 7200.

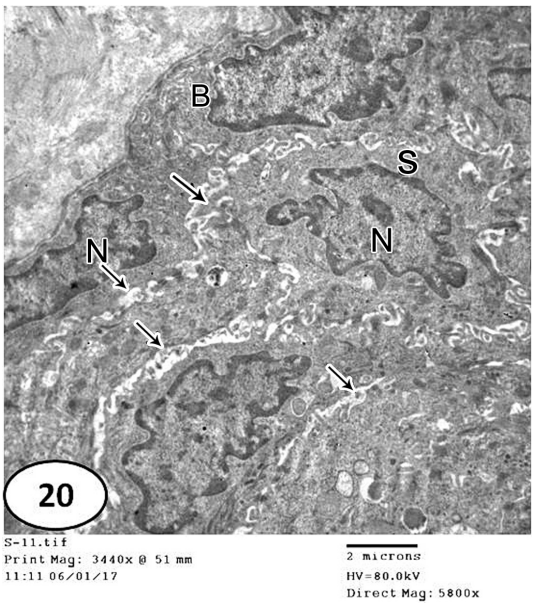

Fig. 20: An electron micrograph of an ultrathin skin section of adult rat (group 2) showing basal (B) and spinous (S) keratinocytes. The nuclei (N) are heterochromatic and highly folded with peripheral chromatin condensation. There is a disruption of desmosomes with an apparent widening in the intercellular space (arrows). EM, X 5800.

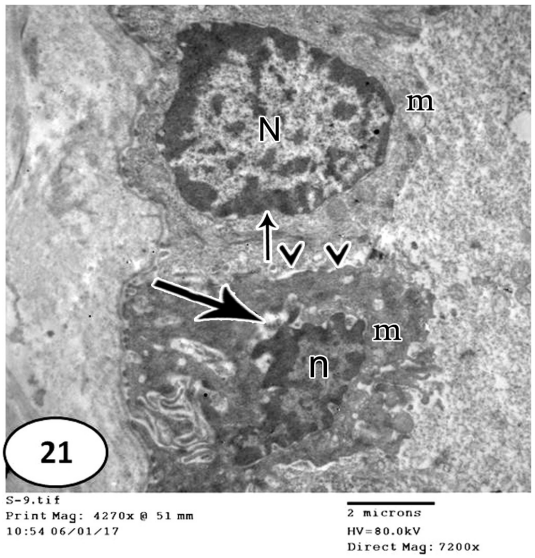

Fig. 21: An electron micrograph of an ultrathin skin section of adult rat (group 2) showing basal keratinocytes. Some cells have nuclei (N) with peripheral chromatin condensation and irregular outline (thin arrow). Other cells have electron dense shrunken, highly folded nucleus (n) with perinuclear halos (thick arrow). Note the vacuolated mitochondria (m) inside the darkly stained cytoplasm. Widened intercellular spaces (arrow heads) with disruption of desmosomal junctions can be seen. TEM, X 7200.

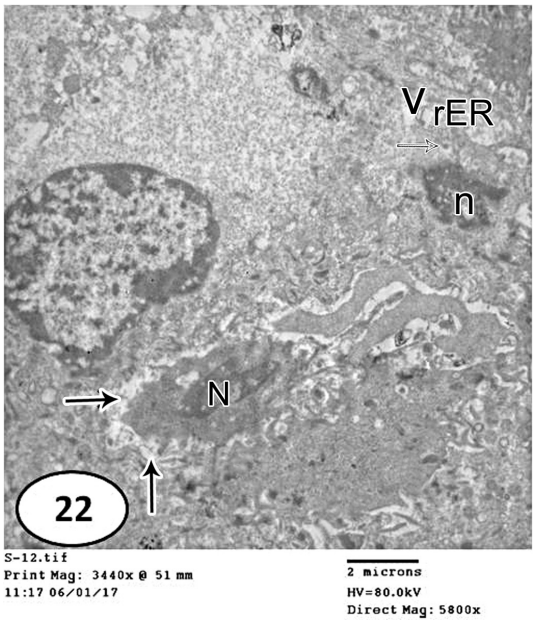

Fig. 22: An electron micrograph of an ultrathin skin section of adult rat (group 2) showing shrunken spinous cell with apoptotic nucleus (N). The cell is surrounded by an extensively wide intercellular space (arrows). Note the adjacent cell with apoptotic nucleus (n). Its cytoplasm reveals vacuolations (V) and dilated cisternae of rough endoplasmic reticulum (rER) with some cisternae containing dense particles (open arrow). TEM, X 5800.

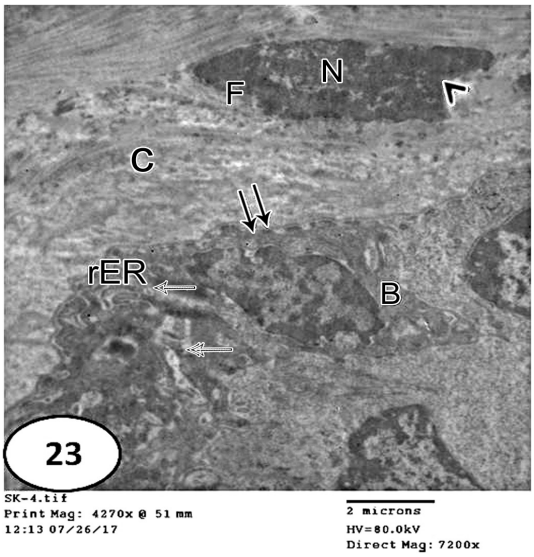

Fig. 23: An electron micrograph of an ultrathin skin section of adult rat (group 2) showing a fibroblast (F) with electron dense, finely granulated nucleus (N), an irregular nuclear membrane (arrow head) with deeply stained scanty cytoplasm. Cellular organelles are not clearly discriminated. Basal keratinocytes (B) with dilated rough endoplasmic reticulum cisternae (rER) containing dense particles (open arrows) are observed overlying the basement membrane (double arrow). Note the underlying disorganized collagen bundles (C). TEM, X 7200.

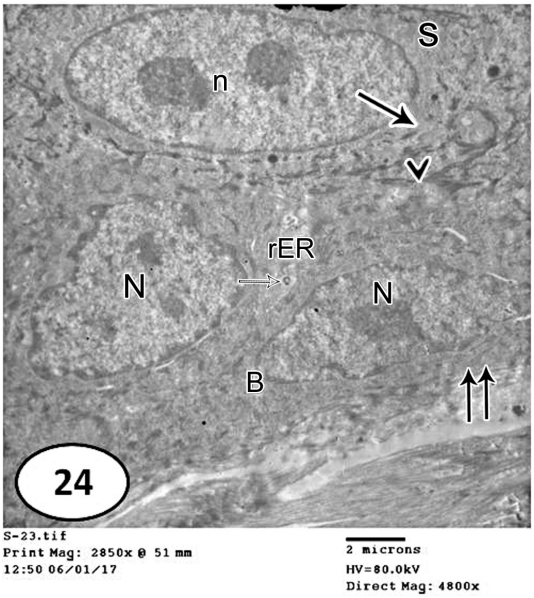

Fig. 24: An electron micrograph of an ultrathin skin section of adult rat (group 3) showing basal keratinocytes (B) resting on the basement membrane (double arrow) with an euchromatic nucleus (N) and a deeply stained cytoplasm which reveals dilated cisternae of rough endoplasmic reticulum (rER) that contain dense particles (open arrow) . The adjacent spinous cells (S) can be seen with oval euchromatic nucleus (n), little amount of tonofilaments (arrow). Note the desmosomes (arrow head) with the adjacent cells. TEM, X4800.

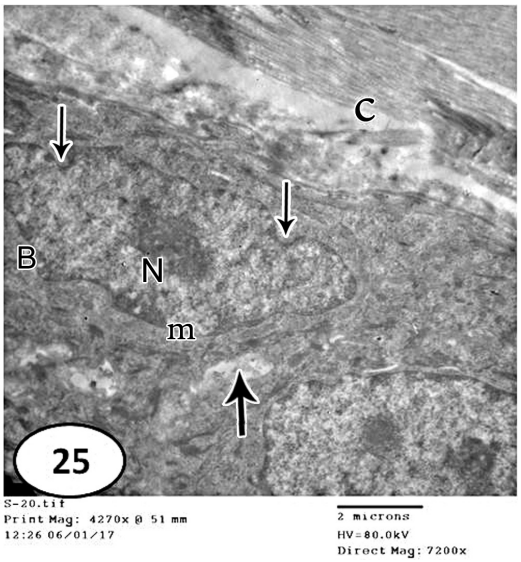

Fig. 25: An electron micrograph of an ultrathin skin section of adult rat (group 3) showing basal keratinocytes (B) with an irregular nucleus (N) which reveals indentation (thin arrows) and mitochondria (m) in the cytoplasm. Widening of the intercellular spaces is still seen (thick arrow). Note the underlying collagen fibers (C) in the dermis. TEM, X 7200.

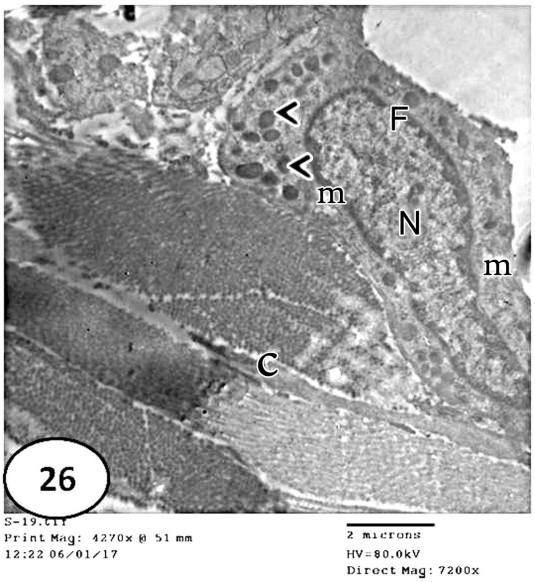

Fig. 26: An electron micrograph of an ultrathin skin section of adult rat (group 3) showing a fibroblast (F) with an oval elongated nucleus (N). Vacuolated mitochondria (m) and many electron dense bodies (arrow heads) could be seen in the cytoplasm. Collagen bundles (C) are observed in the underlying dermis. TEM, X 7200.

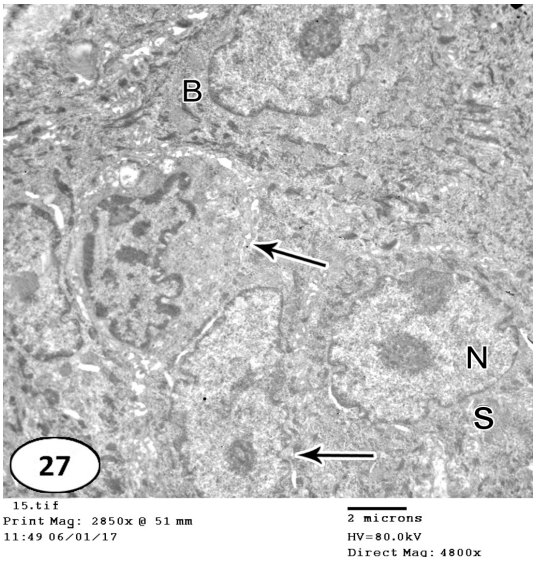

Fig. 27: An electron micrograph of an ultrathin skin section of adult rat (group 4) showing: basal keratinocytes (B) and adjacent spinous cells (S) which reveal euchromatic nuclei (N) and appear nearly similar to the control. Slight widening of the intercellular spaces is noticed in some areas (arrows). TEM, X 4800.

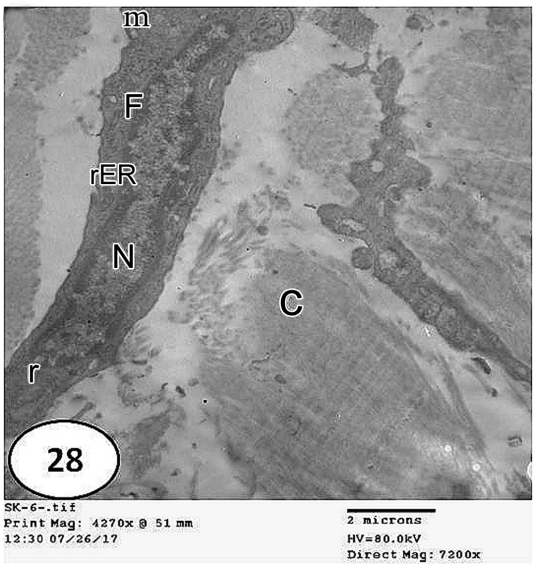

Fig. 28: An electron micrograph of an ultrathin skin section of adult rat (group 4) showing a fibroblast (F) with an oval elongated nucleus (N). The cytoplasm contains rough endoplasmic reticulum (rER) and free ribosomes (r). Some vacuolated mitochondria (m) are seen. Note collagen bundles (C). TEM, X 7200.

Table 1: Mean values of epidermal thickness in the studied groups

Mean±SD	38.54±1.78	15.30±2.50	20.92±1.91	36.73±2.66
Range	36.0-41.1	11.6-19.9	16.7-23.2	31.5-39.5
P-value[1]		0.000*	0.000*	0.131
P-value[2]			0.000*	0.000*
P-value[3]				0.000*

SD: standard deviation
* Statistical significant difference ($P< 0.05$)
1: Comparison with Group 1 - 2: Comparison with Group 2
3: Comparison with Group 3

Table 2: Mean values of area percent of collagen fibers in the studied groups

Area percent	Group 1	Group 2	Group 3	Group 4
Mean±SD	78.47±2.22	48.65±2.75	59.52±2.20	77.27±3.16
Range	75.7-82.0	44.7-52.2	55.2-62.0	73.8-85.2
P-value[1]		0.000*	0.000*	0.199
P-value[2]			0.000*	0.000*
P-value[3]				0.000*

SD: standard deviation
* Statistical significant difference ($P< 0.05$)
1: Comparison with Group 1 - 2: Comparison with Group 2
3: Comparison with Group 3

Table 3: Mean values of area percent BCL-2 expression in the studied groups

Area percent	Group 1	Group 2	Group 3	Group 4
Mean±SD	7.71 ± 0.83	4.55 ± 0.71	7.14 ± 0.82	7.43 ± 0.93
Range	6.3-8.8	3.5-5.7	5.9-8.3	6.0-8.7
P-value[1]		0.000*	0.089	0.570
P-value[2]			0.000*	0.000*
P-value[3]				0.449

SD: standard deviation
* Statistical significant difference ($P< 0.05$)
1: Comparison with Group 1 - 2: Comparison with Group 2
3: Comparison with Group 3

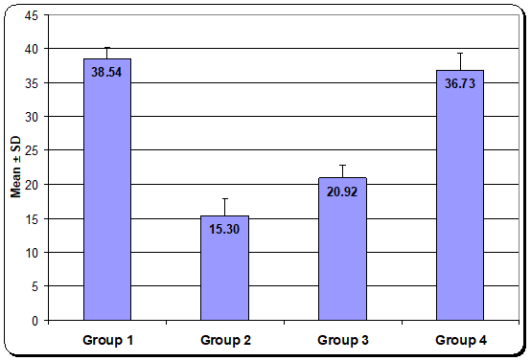

Histogram 1: Mean values of epidermal thickness in the studied groups

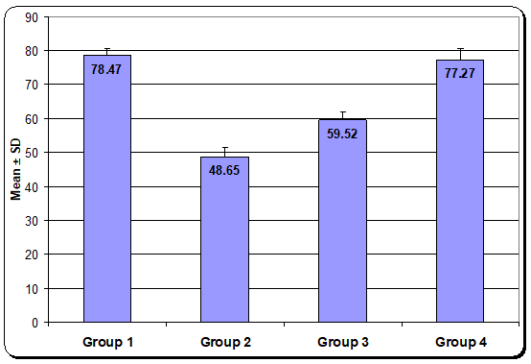

Histogram 2: Mean values of area percent of collagen fibers in the studied groups

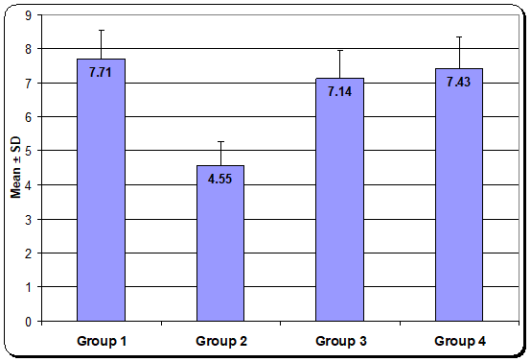

Histogram 3: Mean values of area percent BCL-2 expression in the studied groups

DISCUSSION

This study aimed to evaluate the therapeutic and prophylactic effect of folic acid (FA) against sodium fluoride (NaF) toxicity on the adult male albino rat skin.

Fluoride (F) is a widespread water contaminant that causes a set of serious health problems[20]. It exists in varying amounts in food, water and causes air pollution from numerous industrial operations[21]. Human exposure to fluoride may occur through toothpastes, fluoride additives, and administration of fluoride gel[2].

Fluoride is absorbed and transported through the blood to tissues and organs[21]. Excessive exposure to fluoride may lead to acute poisoning, or chronic intoxication[1]; (Fluorosis) which is due to long term exposure[22].

This study was done on the skin, as it is the biggest mechanoreceptive organ in our body[23]. Meanwhile, it is a major potential route for the absorption of toxic materials encountered in the workplace. Consumer products contain different concentrations of sodium fluoride that may cause symptoms either due to skin, ingestion or inhalation exposure[24].

In NaF treated group, the epidermal thickness was decreased compared to the control. This reduction was confirmed by morphometric results and statistical analysis. At the same time, the epidermal cells showed many signs of degeneration as deeply stained nuclei, pale rarified cytoplasm, expansion of intercellular space, shrunken, irregular nuclei and damaged organelles. These destructive effects of NaF may be due to oxidative stress; this is in harmony with Mansour & Tawfik[25] who stated that there is a relationship between fluoride toxicity and elevated oxidative stress in rats. In addition, Abd EL-aziz *et al*.[4] reported that cell damage and apoptosis due to oxidative stress starts after chronic fluoride exposure.

Hassan & Yousef[26] suggested that oxidative/ nitrosative damage is the major mode of action of fluoride toxicity. The toxic effects of fluoride might be through; formation of free radicals, lipid peroxidation, and modified antioxidant defense systems[27]. Animals treated with fluoride showed altered levels of Glutathione (GSH), Superoxide dismutase (SOD) and Total Anti-oxidant Capacity (TAC) which augment the accumulation of free radicals[28]. Meanwhile, Hassan &Yousef[26] reported that fluoride induces nitric oxide (No) which in turn inhibits mitochondrial respiration that leads to damage of cellular components.

Furthermore, in agreement with this study Prado *et al*.[7] found that keratinocytes lost their stratified appearance and deduced that, fluoride could affect cell differentiation, which explain fluoride-induced tissue disturbances and disorganization.

Masson's trichrome stain in NaF treated group showed a significant decrease, fragmentation and disorganization of collagen fibers. This was confirmed by morphometric and statistical results which showed a significant decrease in area% of collagen fibers in the treated group comparing to control. These results were in harmony with Ghafeer *et al*.[23] who reported that, the decrease in the dermal collagen might be due protease enzymes originated from inflammatory cells, as collagenase enzyme of neutrophils or may be due to reduction of biosynthesis of collagen molecules[29]. Susheela & Mukerjee[30] declared that, Fluorosis is not only a disease of bone and tooth, but it also affects the non-osseous tissues.

Collagen is a structural constituent of osseus and non-osseous tissues and its biosynthesis is greatly impaired due to fluoride intoxication. It increases the non-collagen proteins as proteoglycans and glucosaminoglycans so, speeding up the skin aging[1]. Sharma[31] reported that the hydroxylation of proline to hydroxyproline is intervened by fluoride. Therefore collagen breakdown in many organs as bone, muscle, skin, lungs, kidney and trachea may be due to disturbance in the formation of collagen fibers after fluoride exposure[30]. Susheela and Sharma[8] declared that fluoride induced reduction in the aldehyde content of bone, tendon (collagen type I) and skin (collagen type I + Ill) tissues.

Bcl-2 is an antiapoptotic protein that prevents apoptosis in response to various stimuli. It plays an important role in regulating cell survival and apoptosis. Bcl-2 inhibits apoptosis by preventing the release of cytochrome C[12]. In this study, Bcl-2 showed weak immunoreactivity in NaF treated group and these results were confirmed by morphometric measurements which showed a significant decrease in area% of Bcl-2 expression in the treated group as compared to the control. The present results were augmented by Xu *et al*.[32] who found that NaF induces apoptosis via Bcl-2 suppression.

It has been suggested that alterations in apoptosis may be due to age-associated changes. The epidermis in aged animals showed a decreased thickness and most keratinocytes appeared with deeply stained small nuclei surrounded by pale clear cytoplasm with increased interspaces between disorganized collagen fibers[33]. In contrast, overexpression of Bcl-2 causes accumulation of cells and may leads to neoplasia[12].

Folic acid (FA) is the synthetic form of folate (vitamin B9)[9]. It is present in a variety of foods[34].

The findings of this study demonstrated the efficiency of FA in combating the free radical interposed oxidative insult produced by sodium fluoride (NaF). There was a relative improvement in the dermal and epidermal structures in group 3. Meanwhile, group 4 revealed preservation of the skin architecture to a great extent. This was evidenced by the light and the electron microscopic examination and confirmed by statistical results of epidermal thickness, area% of collagen fibers and of Bcl-2 expression. The current results were in agreement with the studies of Barichello *et al*.[35] who imputed these changes to the free radical scavenging properties and possible antioxidant activity of FA. It was stated that FA is a potent antioxidant[10] and it enhances the cell existence

and inhibits apoptosis[11]. Koul *et al*.[36] revealed that, FA suppressed the expression of ornithine decarboxylase (ODC) in skin and activity of serum lactate dehydrogenase, suggesting inhibitory effects on cell damage. Stanhewicz *et al*.[37] reported that, Folic acid and its metabolite, 5-methyltetrahydrofolate (5-MTHF), may improve vessel function. So, repeated folic acid supplementation would ameliorate the cutaneous microvascular function.

CONCLUSION

The present study provided a valuable insight on the role of FA in alleviation the toxic effects of sodium fluoride on the skin in addition to its beneficial prophylactic role.

CONFLICT OF INTERESTS

There are no conflicts of interest.

REFERENCES

1. Machoy-Mokrzyńska A. Fluorine as a factor in premature aging. Annales Academiae Medicae Stetinensis. 2004; 50(1):9-13.
2. Atamaca N, Atamaca HT, Kanici A and Anteplioglu T. Protective effect of resveratrol on sodium fluoride-induced oxidative stress, hepatotoxicity and neurotoxicity in rats. Food and Chemical Toxicology. 2014; 70: 191-197.
3. Gouri PN, Otilia BJ, Banji D, Ragini M and Pavani B. Fluoride toxicity-a harsh reality. International Research Journal of Pharmacy. 2011; 2: 79-85.
4. Abd El-Aziz EA, Abd El-Haffez AS and Ahmed AM. Memory-Enhancing Effects of Folic Acid against Fluoride-Induced Cognitive Deficits in Adult Male Rats. Medical Journal of Cairo University. 2017; 85(1): 221-234.
5. Thrane EV, Refsnes M, Thoresen GH, Lag M and Schwarze PE. Fluoride-induced apoptosis in epithelial lung cells involves activation of MAP kinases p38 and possibly JNK. Toxicological Sciences. 2001; 61(1):83–91.
6. Partanen S. Inhibition of human renal acid phosphatases by nephrotoxic micromolar concentrations of fluoride. Experimental and Toxicologic Pathology. 2002; 54(3):231–237.
7. Prado E, Wurtz T, Ferbus D, Shabana E, Forest N and Berdal A. Sodium fluoride influences the expression of keratins in cultured keratinocytes. Cell Biology and Toxicology. 2011; 27:69–81. DOI10.1007/ s10565-010-9171-5.
8. Susheela AK, Sharma YD. Effect of Fluoride on collagen cross-links precursors of rabbit tissues. Pharmacology. 1981; 9: 862.
9. Juzeniene A, Grigalavicius M, Ma LW and Juraleviciute M. Folic acid and its photoproducts, 6-formylpterin and pterin-6-carboxylic acid, as generators of reactive oxygen species in skin cells during UVA exposure. Journal of Photochemistry and Photobiology. 2016; 155:116-21.
10. Singh R, Kanwar S S, Sood PK and Nehru B. Beneficial effects of folic acid on enhancement of memory and antioxidant status in aged rat brain. Cellular and Molecular Neurobiology. 2011; 31: 83-91.
11. Cheng F, Lan J, Xia W, Tu C, Chen B, Li S and Pan W. Folic Acid Attenuates Vascular Endothelial Cell Injury Caused by Hypoxia via the Inhibition of ERK1/2/NOX4/ROS Pathway. Cell Biochemistry and Biophysics. 2016; 74: 205- 11.
12. Zidan RA, AbdEl-Haleem MR. Effect of caloric dietary restriction on the structure of aged skin and liver in male mice: a histological and immunohistochemical study. The Egyptian Journal of Histology. 2011; 34:505–517.
13. Desouky MK, Anwar RI and Algaidi SA. Immunohistochemical Expression of Bcl-2 and Microvessel Density in Uterine Fibroids in Saudi Patients. West Indian Medical Journal. 2015; 2(3):121-126.
14. Shanmugam T, Abdulla S, Yakulasamy V, Selvaraj M, Mathan R. A mechanism underlying the neurotoxicity induced by sodium fluoride and its reversal by epigallocatechin gallate in the rat hippocampus: involvement of NrF2/Keap-1 signaling pathway. The Journal of Basic and Applied Zoology. 2018; 79:17
15. Salama AF, Touson EM., Ebrahim WM, Elwan MS. Ameliorating Role of Folic Acid in Eltroxine Induced Hyperthyroid and Oxidative Stress in Rat Cortex, Hypothalamus and Hippocampus. Alexandria Journal of Veterinary Sciences. 2017; 55 (1): 210-216.
16. Bancroft JD, Gamble M. "Theory and practice of Histological Techniques".The 7th edition. Philadelphia: Churchill Livingstone of Elsevier.2013; pp.172-186.

17. Graham L, Orenstein JM. Processing tissue and cells for transmission electron microscopy in diagnostic pathology and research. Nature Protocols. 2007; 2 (10): 2439-2450.
18. Wang E. Senescent human fibroblasts resist programmed cell death and failure to suppress bcl2 is involved. Cancer Research. 1995; 155: 2284–2292.
19. Cattoretti G, Pileri S, Parravicini C, Becker MH, Poggi S, Bifulco C, *et al*. Antigen unmasking on formalin-fixed, paraffin-embedded tissue sections. Journal of Pathology. 1993; 171:83–98.
20. Tiwari H, Rao MV. Curcumin supplementation protects from genotoxic effects of arsenic and fluoride. Food and Chemical Toxicology. 2010; 48:1234–1238.
21. Zhou B, Wang H, Wang J, Zhang J, Yan X and Wang J. Effects of malnutrition and supplemented nutrition on nonspecific immune function changes induced by fluoride in rabbits. Research report Fluoride. 2007; 40(3):169–177.
22. Chouhan S, Flora SJ. Arsenic and fluoride: Two major ground water pollutants. Indian Journal of Experimental Biology. 2010; 48: 666-678.
23. Ghafeer HH, El-Gamal DA, Mohamed NA and Hassanin AI. Histological study of human abdominal skin after repeated pregnancy. The Egyptian Journal of Histology. 2015; 38:41-56.
24. Al-Saggaf SM, Ali SS, Ayuob NN, Batawii AH and Mujalled MI. Histological study on the effect of gasoline on guinea pig epidermis: can flavonoid extract reverse this effect? The Egyptian Journal of Histology. 2011; 34:156–165.
25. Mansour HH, Tawfik SS. Efficacy of lycopene against fluoride toxicity in rats. Pharmaceutical Biology. 2012; 50(6): 707–711.
26. Hassan HA, Yousef MI. Mitigating effects of antioxidant properties of black berry juice on sodium fluoride induced hepatotoxicity and oxidative stress in rats. Food and Chemical Toxicology. 2009; 47, 2332–2337.
27. Danguole Z, Saule U, Julius A, Audra P, Nijole J, and Michal S. Experimental studies on effect of sodium fluoride and nitrate on biochemical parameters in rats. Bulletin of the Veterinary Institute in Pulawy. 2007; 51, 79-82.
28. Hassan HA, Abdel-Aziz AF. Evaluation of free radical-scavenging and anti-oxidant properties of black berry against fluoride toxicity in rats. Food and Chemical Toxicology. 2010; 48: 1999–2004.
29. Sayama A, Soushin T, Okada T, Doi K and Nakayama H. Morphological and biochemical changes during aging and photoaging of the skin of C57BL/6J mice. Journal of Toxicologic Pathology. 2010; 23:133–139.
30. Susheela AK, Mukerjee D. Fluoride poisoning and the Effect of Collagen Biosynthesis of Osseous and Nonosseous Tissue." Toxicological European Research. 1981; 3 (2): 99-104.
31. Sharma YD. Effect of Sodium Fluoride on Collagen Cross-Link Precursors, Toxicological Letters. 1982; Vol. 10, 97-100.
32. Xu H, Jin XQ, Jing L and Li GS. Effect of sodium fluoride on the expression of bcl-2 family and osteopontin in rat renal tubular cells. Biological Trace Element Research. 2006; 109(1):55-60.
33. McCullough JL, Kelly KM. Prevention and treatment of skin aging. Annals of the New York Academy of Sciences. 2006; 1067:323–331.
34. Kim YI. Folate and colorectal cancer: An evidence-based critical review. Molecular Nutrition and Food Research. 2007; 51: 267-92.
35. Barichello T, Generoso JS, Simoes LR, Steckert AV, Moreira AP, Dominguini D, *et al*. Folic acid prevented cognitive impairment in experimental pneumococcal meningitis. Journal of Neural Transmission (Vienna). 2015; 122: 643-651.
36. Koul A, Kaur N and Chugh NA. Folic Acid Modulates DMBA/TPA-Induced Changes in Skin of Mice: A Study Relevant to Carcinogenesis. Journal of Dietary Supplements. 2017; 17:16.
37. Stanhewicz AE, Alexander LM, Kenney WL. Folic acid supplementation improves microvascular function in older adults through nitric oxide-dependent mechanisms. Clinical Science. 2015; 129(2):159-67.

الدورالمحتمل لحمض الفوليك ضد تسمم الجلد المحدث من فلوريد الصوديوم فى ذكور الجرذان البيض البالغة

هبة كمال محمد ورشا إبراهيم أنور
قسم التشريح الأدمي وعلم الأجنة- كلية الطب-جامعة أسيوط

ملخص البحث

الخلفية: تعرض الانسان للفلوريد يحدث من خلال عدة مصادر مثل الطعام, المياه, معجون الأسنان و إضافات الفلورايد. التعرض لتركيزات عاليه من الفلورايد او تركيزات منخفضة لمدة طويلة من الممكن ان يؤدي الي التسمم. خاصية جمع الشوارد الحرة لحمض الفوليك تجعله من أقوي مضادات الأكسدة .علاوة علي ذلك فهو يثبط موت الخلايا المبرمج و يعزز بقاء الخلية.

الهدف من البحث: بحث الدور الوقائى والعلاجى المحتمل لحمض الفوليك ضد تسمم الجلد المحدث بفلوريد الصوديوم فى ذكور الجرذان البالغة.

المواد و الطرق المستخدمة: تم تقسيم عدد 40 من ذكور الجرذان (220-200 جرام) البالغة (عمر 3 شهور) بالتساوى إلى 4 مجموعات (10 في كل مجموعة): مجموعة 1 (مجموعة ضابطة), مجموعة 2 (مجموعة معالجة بفلوريد الصوديوم لمدة 4 أسابيع), مجموعة 3 (مجموعة معالجة بفلوريد الصوديوم لمدة 4 أسابيع و يتبعها حمض الفوليك لمدة 4 أسابيع أخرى), مجموعة 4 (مجموعة معالجة بفلوريد الصوديوم + حمض الفوليك لمدة 4 أسابيع). تم إعطاء فلوريد الصوديوم (25مجم/ كجم من وزن الجسم) و حمض الفوليك (8مجم / كجم من وزن الجسم) يوميا عن طريق الفم. ثم تمت التضحية بالفئران و تم أخذ عينات من جلد الظهرو تمريرها للدراسة الهستولوجية, والهيستوكيميائية مناعية (بروتين Bcl2 المضاد لموت الخلايا المبرمج) و القياسات المورفومترية.

النتائج: أظهرت المجموعة الثانية علامات التحلل في خلايا البشرة, إتساع المساحات بين الخلايا و تدمير العضيات في الخلية. كما لوحظ نقص في سمك طبقة البشرة مع تكسر و إختلال في ترتيب الياف الكولاجين و ضعف التعبير المناعي ل Bcl-2 . و قد أظهرت هذه الدراسة فعالية حمض الفوليك في احداث تحسن نسبى فى تركيب طبقة البشرة و الادمة في المجموعة المعالجة بحمض الفوليك. بينما فى المجموعة المحمية بحمض الفوليك تم المحافظة على تركيب هذه الطبقات .

الخلاصة: حمض الفوليك يقلل من التأثيرات الضارة لفلوريد الصوديوم علي الجلد بالاضافة لتأثيره الوقائي المفيد.